Comparison of flux pinning in Si- and $SiCl_4$-doped MgB_2 superconductors: evidence for coexistence of different pinning mechanisms

2015 Supercond. Sci. Technol. 28 125006

(http://iopscience.iop.org/0953-2048/28/12/125006)

IOP Publishing Superconductor Science and Technology
Supercond. Sci. Technol. 28 (2015) 125006 (6pp) doi:10.1088/0953-2048/28/12/125006

Comparison of flux pinning in Si- and $SiCl_4$-doped MgB_2 superconductors: evidence for coexistence of different pinning mechanisms

S R Ghorbani[1], M Hosseinzadeh[1] and X L Wang[2]

[1] Department of Physics, Ferdowsi University of Mashhad, Mashhad, Iran
[2] Institutes for Superconducting and Electronic Materials, Australian Institute for Innovative Materials, University of Wollongong, Faculty of Engineering, North Wollongong, NSW 2519, Australia

E-mail: sh.ghorbani@um.ac.ir

Received 15 July 2015, revised 8 September 2015
Accepted for publication 24 September 2015
Published 23 October 2015

Abstract

The transport and magnetic properties of 5 wt% nano-Si- and 10 wt% $SiCl_4$-doped MgB_2 have been studied by measuring the resistivity, ρ, critical current density, J_c, irreversibility field, H_{irr}, and upper critical field, H_{c2}. Similar scattering mechanisms have been found for both dopants, which are supported by the results for the critical temperature and the upper critical field. The critical current density and the irreversibility field results indicate that there are different pinning mechanisms for nano-Si- and $SiCl_4$-doped MgB_2. Pinning mechanisms are studied in terms of the different pinning models. It was found that a variety of pinning mechanisms, e.g. normal point pinning, normal surface pinning, and normal volume pinning mechanisms coexist in both types of doped MgB_2. The results show that the contributions of the pinning mechanisms are dependent on the temperature and magnetic field.

Keywords: flux pinning, Si source-doped MgB_2, critical current density

(Some figures may appear in colour only in the online journal)

1. Introduction

MgB_2 compound with the critical temperature of 39 K has been the focus of superconductor research for the past 14 years, due primarily to its potential for practical magnetic and electrical applications such as large-scale superconducting magnets and transmission lines. Although considerable improvements have been made during this period, the application of pure MgB_2 remains limited. This is due to the magnetic field dependence of the critical current density, J_c, which is strongly decreased by increasing applied magnetic field as a result of the relatively weak flux pinning [1]. Efforts to improve the J_c properties in MgB_2 have mostly been focused on enhancing the flux pinning ability by irradiation or chemical doping, which has been considered as the most convenient and effective way, because the dopants can introduce extra electrons or second-phase particles [2, 3].

Carbon-containing dopants, originating from C substitution on B sites in the lattice, induce lattice distortion and provide one more electron at each site, thus enhancing the J_c. Nevertheless, the dimensions and the content of the second phase, the sintering temperature, and the original powder size have to be seriously controlled, since only a small quantity of nanoscale particles induce effective pinning centers. As far as the investigation of pure MgB_2 is concerned, researchers have turned to mechanical milling to refine the grains and irradiation to induce defects, both of which are likewise aimed at improving the pinning effects within the crystal [4, 5].

It has been found [6] that nano-Si slightly reduces the critical temperature, T_c, but it is very effective for improving the J_c in both low and high fields, even though no Si substitution takes place. The J_c values for the nano-Si-doped MgB_2 at temperatures above 20 K were found to be even higher than for C-doped MgB_2 [6]. The inclusion of Si source dopants gives us

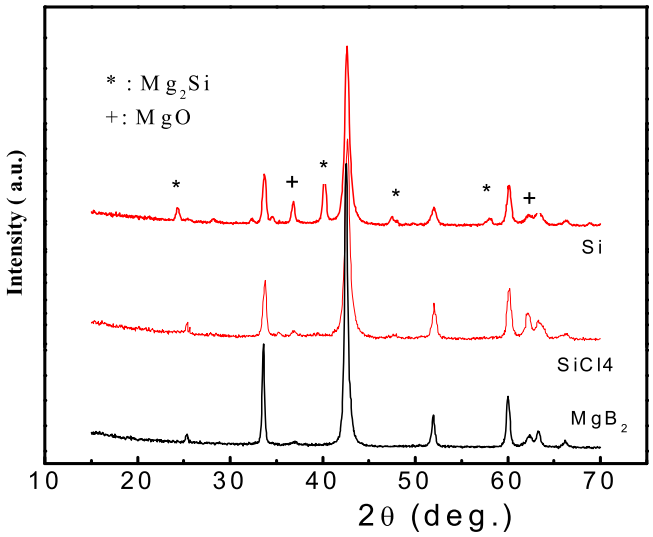

Figure 1. X-ray diffraction patterns of the pure MgB_2, and the nano-Si- and $SiCl_4$-doped MgB_2 samples, with the pure MgB_2 included for comparison.

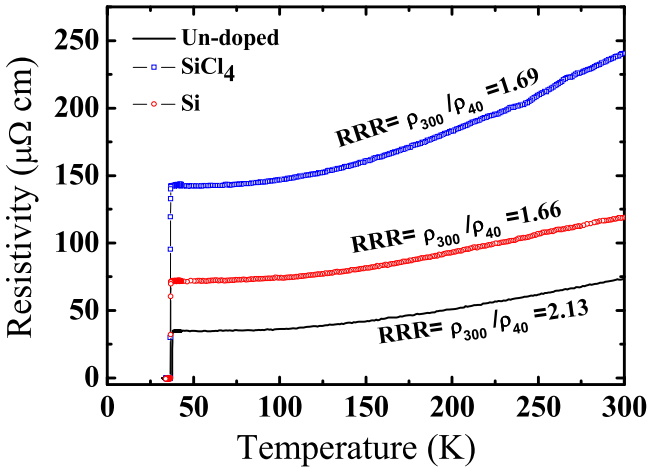

Figure 2. Temperature dependence of the resistivity ρ of the MgB_2 samples with Si and $SiCl_4$ dopants at zero external magnetic field.

an advantage in understanding the flux pinning mechanism compared to the nano-C dopants. This is because Si can introduce point defects inside grains and affect the grain boundaries without any substitution effect, while the nano-C dopants can provide all the effects of point defects, grain boundaries, and substitution on the flux pinning in MgB_2. Therefore, the flux pinning mechanisms are of great interest in Si-source-doped MgB_2 from the point of view of both the fundamental physics and applications. It was also found that $SiCl_4$ doping further enhanced the critical current density, J_c, and the irreversibility field, H_{irr}, in the MgB_2 superconductor above the enhancements from nano-Si doping, while the resistivity, ρ, and the upper critical field, H_{c2}, results show similar behavior for both types of doping. The starting point for the present paper is the question of whether the critical current density behavior can contribute to understanding the similarities and differences between these Si source dopants.

2. Experiment

Polycrystalline MgB_2 samples with 5 wt% nano-Si, and 10 wt% $SiCl_4$ addition, where the appropriate amount of $SiCl_4$ was calculated by considering the molar weight of $SiCl_4$ to correspond to about 10 wt% Si, were prepared at sintering temperatures of 700 and 750 °C for 30 and 10 min in pure Ar gas, respectively, by the standard solid state powder processing technique, which has been well described elsewhere [6, 7]. The microstructures have been previously examined by TEM and the results, which were reported in [6, 7], show that particle sizes of several tens of nanometers in diameter of the MgB_2 are found for both samples. The x-ray diffraction (XRD) patterns, which were recorded using Cu Kα radiation, are presented in figure 1. As can be seen in figure 1, all the samples were crystallized in the MgB_2 structure as the major phase. A few impurity lines of MgO impurity around 9% were observed in the undoped MgB_2 sample. There were also MgO (7%) and Mg_2Si (8%) impurities observed in both doped samples. Therefore, the MgO impurity phase did not depend on doping, in agreement with the results reported previously at sintering temperatures in the 700–750 °C range [6, 7]. The critical temperature T_c was defined as the onset temperature at which diamagnetic properties are observed. The value of T_c was 37 ± 0.30 K for both doped samples, which is slightly lower than for the undoped sample (T_c = 38.0 K), which was sintered at 750 °C. The small drop in the T_c due to the Si-source dopants is caused by both Mg deficiency as a result of the formation of Mg_2Si and the enhanced electron scattering from the Mg_2Si impurity.

Resistivity measurements were carried out on cylindrical samples by using a physical properties measurement system (PPMS, Quantum Design) in the field range from 0 up to 8.7 T. The magnetic hysteresis loops were measured using a magnetic properties measurement system (MPMS, Quantum Design). The critical current density was calculated by using the Bean approximation.

3. Results and discussions

The resistivity ρ as function of temperature for the MgB_2 samples with Si and $SiCl_4$ dopants at zero external magnetic field is shown in figure 2. For comparison, the resistivity of undoped MgB_2 sintered at 750 °C is also added to figure 2. It can be seen that the resistivity depends on the dopant. The results shows that the ρ values at 300 K and 40 K are lower for the nano-Si-doped MgB_2 than for $SiCl_4$ doping. The residual resistivity ratios, RRR ($\rho_{300\ K}/\rho_{40\ K}$), of the MgB_2 samples with different dopants were obtained, which were 2.13 for undoped MgB_2, and 1.66 and 1.69 for Si- and $SiCl_4$-doped MgB_2, respectively. Therefore, these results show that dopants change the scattering processes in MgB_2, although they are similar in both Si-doped and $SiCl_4$-doped MgB_2 samples.

The critical current density $J_c(B)$ results are shown in figure 3 at the temperatures of 20 K for the undoped MgB_2

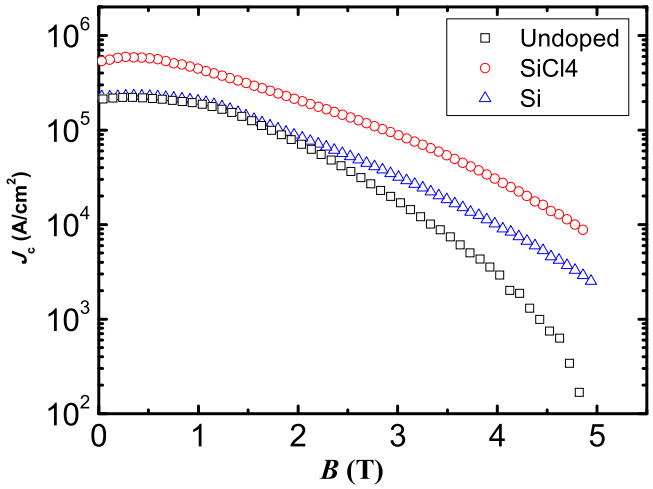

Figure 3. Magnetic dependence of the critical current density for the pure, the 5 wt% Si-doped, and the 10 wt% $SiCl_4$-doped MgB_2 samples at the temperature of 20 K.

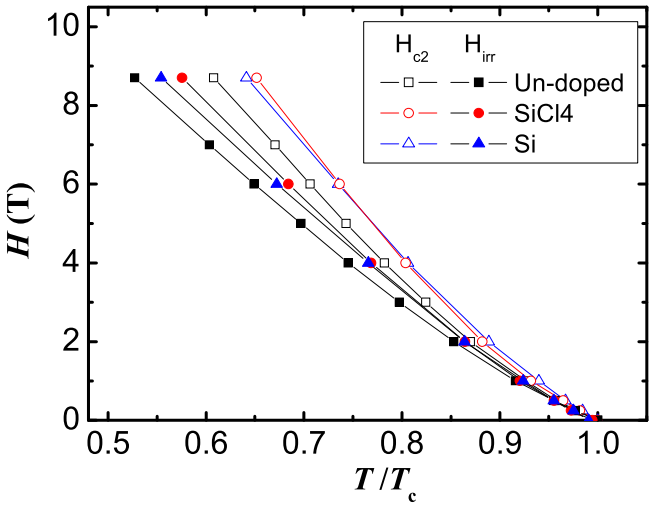

Figure 4. (a) Upper critical field and (b) irreversibility field of the pure, the 5 wt% Si-doped, and the 10 wt% $SiCl_4$-doped MgB_2 as functions of temperature.

and for both the nano-Si- and $SiCl_4$-doped MgB_2 samples. For all the samples, the J_c initially shows a plateau at low field and then begins to decrease quickly once the field reaches the crossover field from the single vortex to the small bundle pinning regime. The $J_c(B)$ values for the undoped MgB_2 and the nano-Si-doped MgB_2 are the same at magnetic fields smaller than 2 T, although further increasing the field results in a faster drop in J_c for the undoped MgB_2 than for the doped samples. As can be seen in figure 3, the $SiCl_4$ doping improves the J_c over the whole range of studied magnetic fields. Why does the $SiCl_4$ doping improve the critical current more than the nano-Si doping? Tentative answers to these questions might be found along the following lines.

So far, it has been widely accepted that partial occupation of the B sites by dopants such as carbon causes stronger intra-band electron scattering in the σ-band than it does in the π-band at high temperature, which leads to a positive curvature of H_{c2} at temperatures close to T_c and therefore enhances H_{c2} significantly. In addition, it was pointed out that the modification of intra-band and inter-band scattering in both the σ- and the π-bands can lead to high H_{c2} [8]. Figure 4 shows the normalized temperature dependence of H_{c2} and H_{irr}, which were obtained from the 90% and 10% values of their corresponding resistivity transitions. Significantly enhanced H_{irr} and H_{c2} are clearly observed for both the nano-Si-doped and the $SiCl_4$-doped MgB_2 samples. The results indicate that the doped MgB_2 samples have higher H_{irr} values compared to the undoped sample. The above results also reveal that H_{c2} does not depend on the dopant, which is in good agreement with the RRR results for both Si-source dopants, as mentioned above, while H_{irr} does. Therefore, the enhancement of in-field J_c or H_{irr} by $SiCl_4$ is not caused by the enhancement of H_{c2}, but is rather due to the introduction of more effective pinning centers compared to those in the nano-Si-doped MgB_2 sample.

It has been pointed out [9] that there are two predominant mechanisms of core pinning, i.e. $\delta\ell$ pinning, which comes from spatial variation in the charge carrier mean free path, ℓ, and δT_c pinning due to randomly distributed spatial variation in T_c, which result in different temperature dependences of the critical current density in the single-vortex pinning regime, J_{sv}. In the framework of collective pinning theory [9], it was found [10] that both $\delta\ell$ pinning and δT_c pinning coexist in the nano-Si-doped MgB_2 sample, although their contributions are strongly temperature dependent. The $\delta\ell$ pinning was dominant at low temperatures and was suppressed completely at temperatures close to the critical temperature, T_c, where the δT_c pinning mechanism was dominant. It was also reported [7] that the $\delta\ell$ pinning mechanism, i.e. spatial variation in the charge-carrier mean free path, was responsible for the flux-pinning mechanism in the $SiCl_4$-doped MgB_2. In order to understand the nature of the pinning mechanisms in more detail, it is useful to study the variation of the vortex pinning force density, $F_p = J_c \times B$, with the field. The normalized pinning force density $\left(f_p = F_p/F_p^{max}\right)$ is a function of the reduced field ($b = H/H_{max}$), where H_{max} is the magnetic field at the maximum of F_p, for both nano-Si- and $SiCl_4$-doped MgB_2. Figure 5 shows the results. For $SiCl_4$-doped MgB_2 (figure 5(b)), close to $H/H_{max} = 1$ the $T = 22$ K data have a noticeable deviation from other temperatures. This suggest that the pinning mechanism is perhaps different for $T = 22$ K. As can be seen in figure 5, the scaling behavior would not be accessible at higher temperatures. Otherwise, scaling was achieved by the following magnetic field dependence for f_p, which has been inferred by Higuchi *et al* [11]:

$$f_{pp} = \frac{9}{4}b\left(1 - \frac{b}{3}\right)^2: \text{ for normal point pinning} \quad (1)$$

$$f_{ps} = \frac{25}{16}\sqrt{b}\left(1 - \frac{b}{5}\right)^2: \text{ for surface (grain boundary) pinning} \quad (2)$$

$$f_{pk} = 3b^2\left(1 - \frac{2b}{3}\right): \text{ for } \Delta\kappa \text{ pinning.} \quad (3)$$

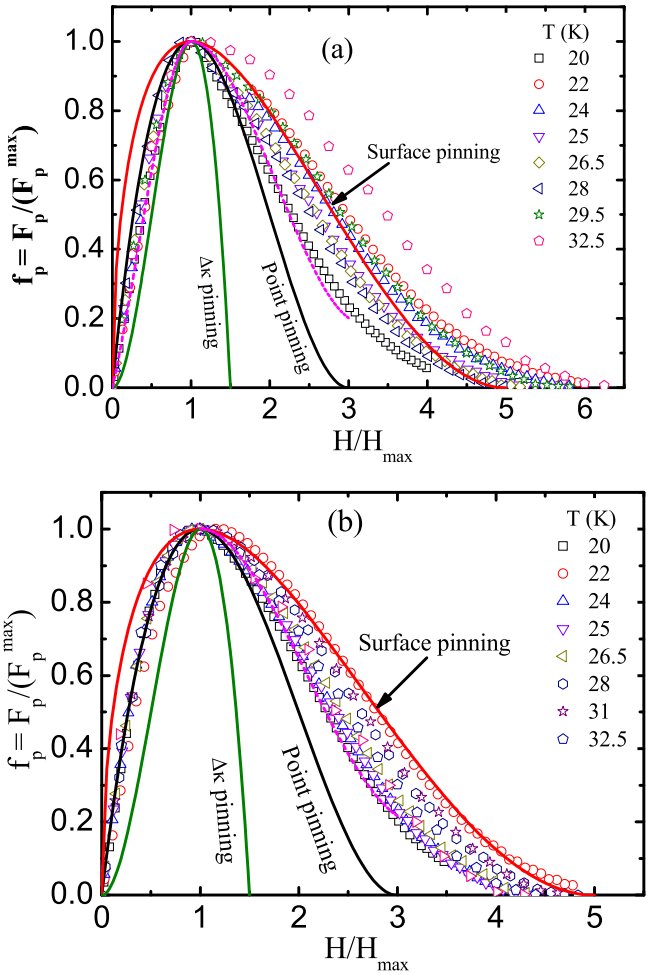

Figure 5. Magnetic field dependence of the reduced pinning force f_p over the temperature range of 20–34 K for (a) the nano-Si-doped MgB_2, and (b) the $SiCl_4$-doped MgB_2.

The fitting results are shown by the solid curves in figures 5(a) and (b). As can be seen in figure 5, the experimental data are not in agreement with any one of the three mechanisms, the point pinning f_{pp}, the surface pinning f_{ps}, and the $\Delta\kappa$ volume pinning f_{pk}, for either dopant. For the nano-Si-doped MgB_2, the experimental data are located between the theoretical curves for $\Delta\kappa$ pinning and point pinning at normalized magnetic fields smaller than b_{max}, while in the reduced magnetic field up to $b = 4$, the dominant pinning mechanism is roughly surface pinning, and at some temperatures, the experimental data are located between the curves for surface pinning and point pinning. Therefore, it seems that some contribution from point pinning may be present in addition to surface pinning. At reduced magnetic fields higher than $b = 4$, the experimental data deviate from the scaling that was suggested by Higuchi *et al* [11].

As can be seen in figure 5(b) for the $SiCl_4$-doped MgB_2, the experimental data are in good agreement with the point pinning mechanism f_{pp} in magnetic fields lower than b_{max}. At normalized magnetic fields above b_{max}, the experimental data are located almost exactly between the curves for surface pinning and point pinning, while at the temperature of 22 K, the experimental data are in good agreement with the surface pinning mechanism f_{ps}. There is no contribution from the $\Delta\kappa$ pinning f_{pk} mechanism for $SiCl_4$ doping. Thus, it seems that the pinning mechanisms are different for the two Si-source dopants.

To investigate further the real pinning mechanisms of MgB_2 doped with Si-source dopants, the normalized pinning force density data was analyzed by combining the contributions from all the mechanisms, the point pinning f_{pp}, the surface pinning f_{ps}, and the $\Delta\kappa$ pinning f_{pk} mechanisms, within the following expression:

$$f_p = a_p f_{pp} + a_s f_{ps} + a_k f_{pk} \tag{4}$$

where a_p, a_s, and a_k are fitting parameters, which represent the point pinning, the surface pinning, and the $\Delta\kappa$ pinning effects, respectively, with $a_p + a_s + a_k = 1$. In this case, the best fitting includes the contributions from point pinning a_p, surface pinning a_s, and $\Delta\kappa$ pinning a_k. The dashed curves through the data in figure 5 exemplify the results for the temperature of 20 K. Results for the pinning contributions are shown in figure 6. As can be seen in the upper panel of figure 6(a), both the point pinning and the $\Delta\kappa$ pinning mechanism coexist in nano-Si-doped MgB_2 at $H < H_{max}$, while there is no contribution from the surface pinning; however, which pinning mechanism is dominant depends on the temperature range. More importantly, the pinning mechanisms change at $H > H_{max}$. From the lower panel of figure 6(a), one can clearly see that the surface pinning has become dominant, and there is no contribution from the $\Delta\kappa$ pinning mechanism. For $SiCl_4$-doped MgB_2 samples, the point pinning is the dominant mechanism, as mentioned above, and the other pinning mechanisms do not contribute at $H < H_{max}$. In figure 6(b) the contributions of the individual pinning mechanisms for $SiCl_4$-doped MgB_2 as a function of temperature are compared at $H > H_{max}$. The $\Delta\kappa$ pinning mechanism does not contribute to the pinning force, but both the point pinning and the surface pinning mechanisms coexist and their contributions depend on temperature. The results clearly show that the surface pinning becomes dominant at temperatures higher than 25 K.

For the scaling, the Dew-Hughes model [12] is usually employed as a single pinning function,

$$F_p = Ah^p(1 - h)^q, \tag{5}$$

where A is a coefficient associated with the material properties, $h = H/H_{irr}$ is the reduced magnetic field, and p and q are parameters that depend on the pinning mechanisms. In this model $p = 0$ and $q = 2$ describe normal-volume pinning (nvp); $p = 1/2$ and $q = 2$ describe normal-surface pinning (nsp); finally, $p = 1$ and $q = 2$ describe normal-point pinning (npp).The maximum of F_p is

$$F_{p,\,max} = A\left[h^p(1 - h)^q\right]_{max}. \tag{6}$$

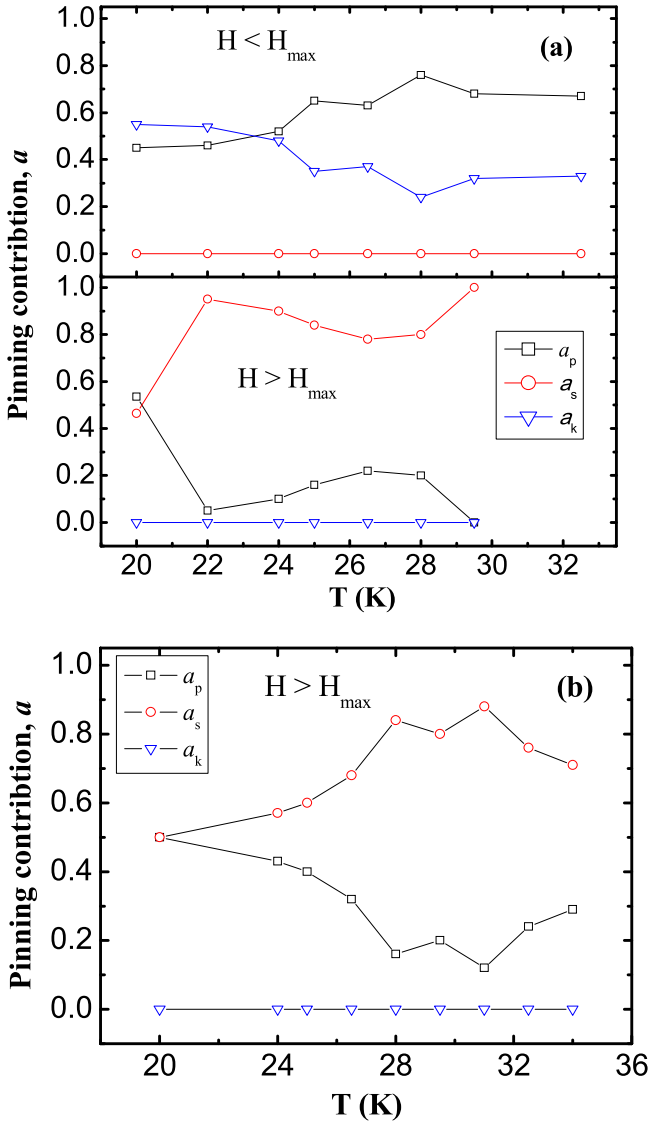

Figure 6. Temperature dependence of the contributions of the point pinning a_p, the surface pinning a_s, and the $\Delta\kappa$ pinning a_k mechanisms for (a) nano-Si doping, and (b) $SiCl_4$ doping.

Therefore,

$$f_p(h) = \frac{F_p}{F_{p,\,max}} = \frac{Ah^p(1-h)^q}{A\left[h^p(1-h)^q\right]_{max}} = \frac{h^p(1-h)^q}{\left[h^p(1-h)^q\right]_{max}} \tag{7}$$

where the maximum of $F_p(h)$ occurs at $h_{max} = p/(p+q)$. Figure 6 shows the results of $f_p(h)$ as a function of reduced field $h = H/H_{irr}$ for various temperatures. The value of H_{irr} was determined by the $J_c = 100\ A\ cm^{-2}$ criterion. It can be seen in figure 7 that the experimental data lie between master curves of the normal point, normal surface, and normal volume pinning for reduced fields larger than h_{max}. Nevertheless, for $h < h_{max}$, $\delta\kappa$ volume pinning may have an effect on the flux pinning, especially for the Si-doped sample. That can be due to lattice imperfections caused by Mg deficiency that arises from the formation of Mg-containing impurities in the form of MgO and $MgSi_4$. The $\delta\kappa$ pinning centers are

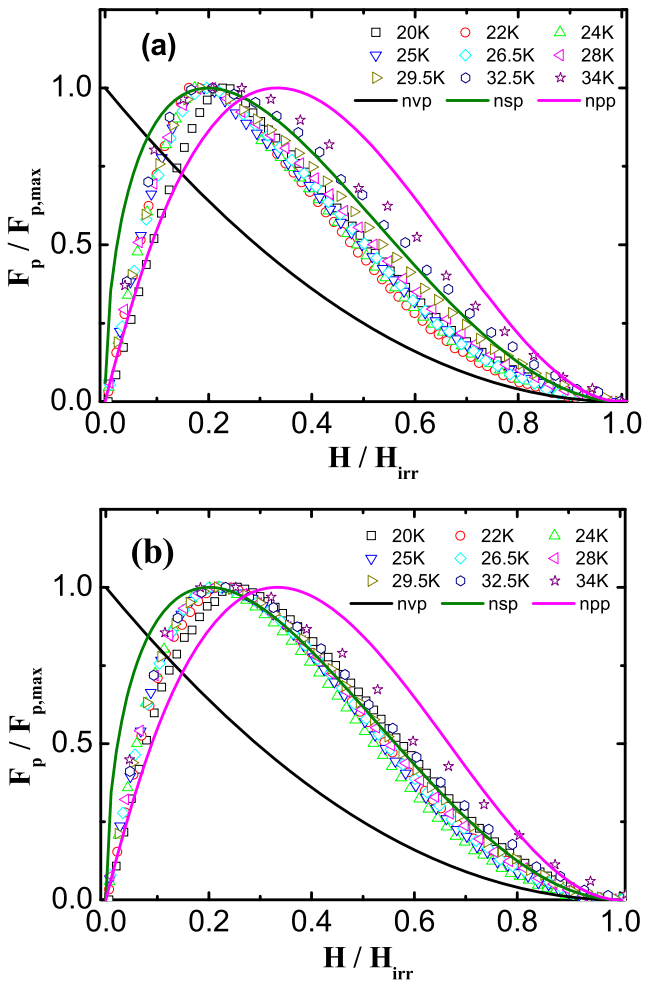

Figure 7. Scaling behavior for (a) the nano-Si-doped MgB_2, and (b) the $SiCl_4$-doped MgB_2.

regions with a lower thermodynamic critical field, H_c. This is because in the core interaction, the pinning potential is proportional to $H_c^2 - H_c'^2$, where H_c' is the thermodynamic critical field of the pinning center [13]. Thus, for $H_c > H_c'$, the pinning potential may be negative, so based on the Ginzburg–Landau theory, where $H_c \propto (T_c - T)$ and $H_{c2} = \sqrt{2}\,\kappa H_c$ [14], the increasing temperature and magnetic field may change the pinning mechanism. As can be seen in figure 7, the $SiCl_4$-doped sample almost follows normal surface pinning, which originates from the grain boundaries, at all temperatures except for 34 K. For the Si-doped sample, however, it seems that there is some contribution from normal volume pinning due to impurities, except for 34 K in reduced fields of $h > h_{max}$. At $h > h_{max}$, the normal volume pinning contribution can be explained in two ways: (1) when the magnetic field is increased, the $\delta\kappa$ volume pinning centers may be converted to normal volume pinning centers; (2) with increasing magnetic field, more flux vortices penetrate to the sample, and the inter-flux-vortex spacing, d, becomes shorter compared to the dimensions of the Mg_2Si particles, which had acted as normal volume pinning centers. These results are supported by microstructure studies of $SiCl_4$-doped MgB_2 samples by transmission electron microscopy (TEM) [6, 7],

where it was found that the size of the Mg_2Si particles is greater relative to the MgO ones. Finally, it can also be found from figure 6 that h_{max} is 0.19 ± 0.03 and 0.22 ± 0.02 for the nano-Si- and $SiCl_4$-doped MgB_2, respectively. These results indicate that normal surface pinning that originates from grain boundaries may be the dominant pinning mechanism, but further details behind this cannot be inferred from this scaling behavior.

In conclusion, the critical temperature and the upper critical field results suggest similar scattering mechanisms for both dopants. It was found that $SiCl_4$ doping improves the critical current density and the irreversibility field more than nano-Si doping in MgB_2, which indicates that the $SiCl_4$ produces stronger and more plentiful pinning centers, which induce different pinning mechanisms. Studies of the pinning mechanisms in terms of the different pinning models indicate that a variety of pinning mechanisms, e.g. normal point pinning, normal surface pinning, and normal volume pinning mechanisms, coexist in both types of doped MgB_2. The results show that the contributions of the pinning mechanisms depend on the temperature and magnetic field.

Acknowledgments

The work was supported by the Ferdowsi University of Mashhad.

References

[1] Finnemore D K, Ostenson J E, Bud'ko S L, Lapertot G and Canfield P C 2001 *Phys. Rev. Lett.* **86** 2420
[2] Dou S X *et al* 2007 *Phys. Rev. Lett.* **98** 097002
[3] Berenov A, Serquis A, Zhao X Z, Zhu Y T, Peterson D E, Bugoslavsky Y, Yates K A, Blamire M G, Cohen L F and MacManus-Driscoll J L 2004 *Supercond. Sci. Technol.* **17** 1093
[4] Perner O, Eckert J, Hässler W, Fischer C, Müller K H, Fuchs G, Holzapfel B and Schultz L 2004 *Supercond. Sci. Technol.* **17** 1148
[5] Eisterer M, Zehetmayer M, Tonies S, Weber H W, Kambara M, Babu N H, Cardwell D A and Greenwood L R 2002 *Supercond. Sci. Technol.* **15** L9
[6] Wang X L, Zhou S H, Qin M J, Munroe P R, Soltanian S, Liu H K and Dou S X 2003 *Physica* C **385** 461
Wang X L, Soltanian S, James M, Qin M J, Horvat J, Yao Q W, Liu Q W and Dou S X 2004 *Physica* C **408–10** 63
[7] Wang X L, Dou S X, Hossain M S A, Cheng Z X, Liao X Z, Ghorbani S R, Yao Q W, Kim J H and Silver T 2010 *Phys. Rev.* B **81** 224514
[8] Gurevich A 2003 *Phys. Rev.* B **67** 184515
[9] Blatter G, Feigel'man M V, Geshkenbein V B, Larkin A I and Vinokur V M 1994 *Rev. Mod. Phys.* **66** 1125
[10] Ghorbani S R, Wang X L, Hossain M S A, Dou S X and Lee S I 2010 *Supercond. Sci. Technol.* **23** 025019
[11] Higuchi T, Yoo S I and Murakami M 1999 *Phys. Rev.* B **59** 1514
[12] Dew-Hughes D 1974 *Phil. Mag.* **30** 293
[13] Ketterson J B and Song S N S 1999 *Superconductivity* (Cambridge: Cambridge University Press)
[14] Annet J F 2004 *Superconductivity, Superfluids, and Condensate* (Oxford: Oxford University Press)